Granular Matter (2009) 11:221–236
DOI 10.1007/s10035-009-0138-2

Influence of relative density on granular materials behavior: DEM simulations of triaxial tests

Christophe Salot · Philippe Gotteland · Pascal Villard

Received: 29 August 2007 / Published online: 30 April 2009

Abstract The rheological behavior of non-cohesive soils results from the arrangement and complex geometry of the grains. Numerical models based on discrete element modeling provides an opportunity to understand these phenomena while considering the discrete elements with a similar shape to that of the grains the soil is composed of. However, dealing with realistic shapes would lead to a prohibitive calculation cost. In a macroscopic modeling approach, simplification of the discrete elements' shape can be done as long as the model can predict experimental results. Since the intrinsic non-convex geometry property of real grains seems to play a major role on the response of the granular medium, it is thus possible to keep this geometrical feature by using cluster of spherical discrete elements, which has the advantage to reduce dramatically the computation cost. Since the porosities found experimentally could not always be obtained with the numerical model—owing to the huge difference in shape, the notion of relative density, which requires a search for minimum and maximum porosities for the model, was chosen to compare the experimental and numerical results. Comparing the numerical simulations with the experimental triaxial tests conducted with relative densities and different confining pressures shows that the model is able to predict the experimental results.

Keywords Granular materials · Discrete element model · Shape of elements · Porosity · Triaxial tests

C. Salot · P. Gotteland (✉) · P. Villard
Laboratoire 3S-R, UJF, CNRS, INP, UMR,
Grenoble Universités, Grenoble, France
e-mail: philippe.gotteland@hmg.inpg.fr

1 Introduction

Granular materials are important components of a geotechnical structure. They are used alone or in combination with various other materials (reinforcement, drains, or recycled materials) to modify its mechanical or hydraulic behavior. The arrangement and interlocking of the soil grains have a decisive impact on the mechanical behavior of the granular assembly and therefore on the behavior of the structure. In many of today's applications, engineers do not have the tools available that allow them to take the changes in density of granular materials into consideration in the designing methods used.

This is particularly true in the evaluation of the liquefaction strength of soils [1], reclaimed fill [2], innovative structures composed of combinations of materials with various mechanical characteristics such as tire–reinforced sand mixtures [3], or structures that are subjected to strong impacts such as protective barriers against rockfall [4].

To remedy these shortcomings, a numerical model is proposed, based on the discrete element method that takes into consideration the porosity of the material. The numerical model is defined by a limited number of parameters and integrates simple element shapes. The ability of the numerical model to reproduce the mechanical behavior of a granular assembly with different porosities was validated by comparison with axisymmetric triaxial compression tests on real sand.

The discrete element method developed by Cundall and Strack [5] is used to study the behavior of composite materials composed basically of granular materials [6,7]. Contrary to the models based on the finite element method, the discrete element modeling (DEM) can model the complex behavior of a granular medium with few parameters. The discrete nature of the DEM models can also highlight localization

phenomena. In the solution process there are two successive alternating computation phases at each time step:

- the determination of the normal contact and tangential forces between two interacting elements, obtained from a contact law,
- the calculation of the displacement of each element through a dual integration of Newton's second law of motion.

Classical models are based on the definition of spherical discrete elements to optimize computation times during contact detection. These models cannot quantitatively reproduce the shear strength of a granular soil subjected to triaxial tests [8] given the rolling mechanisms that may develop with the spherical elements. As Matsushima and Saomoto [9] have emphasized, elements that are more angular may cause an increase in shear strength.

Several methods have been proposed to correct grain rolling: they are based either on the definition of non-spherical elements or they integrate contact laws that result in partially or totally blocking the rotations.

Simple 2D models have been proposed on the basis of elliptical convex elements [10–14], polygon-shaped elements [15–21], superquadrics [22] or non-round elements defined by circular segments [23,24]. More sophisticated shapes are obtained in 2D using a bundle of overlapping or jointed discs [25–29]. In the same way, 3D models based on ellipsoids [30–33], polyhedrons [34–37], or overlapping or jointed spheres [9,38–42] are used.

However, it seems that the convexity of the elements composed of spheres supports rolling, which is the source of the low level of resistance achieved by the samples during biaxial simulation. Nevertheless, non-convex elements have many points of contact, which enable the transfer of a resistance moment even in the absence of frictional forces. This moment tends to increase the overall resistance of the granular assembly [43]. O'Sullivan and Bray [41] explain that this increase in resistance caused by stabilization increases force chains.

Specific algorithms have been developed to enable a closer approximation of the true shape of the grains of soil by using 2D [29] and 3D [9,37,42] clusters of spheres. These models require a high number of spherical elements, which affects the computation time, without realistically coming close to the true shape of the grain.

An alternative would be to limit the rotation of the elements. Calvetti et al. [44] impede all rotation of the elements and partially reproduce the mechanical behavior of sands with biaxial solicitations, whereas Iwashita and Oda [45] modified the traditional contact laws by introducing a resistance to rolling.

To optimize computation time, for this study simple contact laws and elements made up of inseparable spheres that can be either interlocked or not, were considered. These elements are non-convex and not limited in rotation. This global approach is used to reproduce the behavior of real soil as accurately as possible without having to precisely describe the geometry of the grains and the granular distribution of the medium to be modeled.

To validate this approach, numerical simulations of the axisymmetric triaxial compression tests were compared to experimental results. The model was calibrated on one test, carried out at a given porosity and under a confinement stress. Once it was calibrated, the model was tested for various porosities and different confinements.

In the calibration stage, different shapes of discrete elements and several sets of micromechanical parameters were tested. The concave aspect of these elements generates numerical samples of porosity ranges that are well above those of the experimental samples. The experimental and numerical results therefore cannot be compared at the same porosity. The notion of relative density makes this comparison possible but requires that minimum and maximum porosities of the sample be defined. A procedure to determine these relative densities within the model is presented.

2 Presentation of the numerical model

2.1 Interaction laws

The code used for this study is the SDEC software [46]. It is based on the molecular dynamics method and integrates 3D sphere assemblies. The spherical shape of the basic elements enables the computation time to be optimized in terms of detecting contacts, since the spheres interact with contacts that are assumed to be punctual.

The macroscopic behavior of granular assemblies is a function of the geometry of the elements, their initial arrangement, and three intrinsic parameters (E_c, α and φ_μ) of the material, independent of the size of the elements.

Coefficient α and the normal contact modulus E_c account for the elastic behavior of the granular assembly. The microscopic friction angle φ_μ characterizes the failure criterion between the elements.

With each sphere of radius R_i normal stiffness $k_{n,i}$ and tangential stiffness $k_{s,i}$ are associated defined by Eqs. 1 and 2 with parameters E_c and α.

The normal force F_n exerted between the two spheres i and j is related to the interpenetration of spheres d_n according to Eq. 3. Therefore, no tensile strength is possible between the elements. At each time step, the tangential force is incremented by ΔF_s. The variation ΔF_s of the tangential force F_s is defined based on the tangential displacement increment Δd_s by Eq. 4. A friction law of the Coulomb type is used. At each contact, it limited the absolute value of the tangential

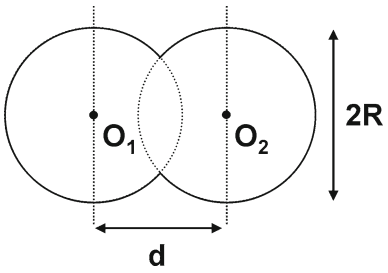

Fig. 1 Definition of the parameters d and R for two spheres making up one clumped element

force to a fraction of the normal force (Eq. 5).

$$k_{n,i} = E_c \cdot R_i \tag{1}$$

$$k_{s,i} = \alpha \cdot k_{n,i} \tag{2}$$

$$F_n = K_n \cdot d_n \quad \text{with} \quad K_n = \frac{k_{n,i} \cdot k_{n,j}}{k_{n,i} + k_{n,j}} \tag{3}$$

$$\Delta F_s = K_s \cdot \Delta d_s \quad \text{with} \quad K_s = \frac{k_{s,i} \cdot k_{s,j}}{k_{s,i} + k_{s,j}} = \alpha \cdot K_n \tag{4}$$

$$|F_s| \leq \tan\left(\varphi_\mu\right) \cdot F_n \tag{5}$$

The conditions at the boundaries of the model are controlled by rigid walls without any friction. These walls impose displacements or forces on the sample through a controlled procedure. The contact stress between a sphere i and a wall is normal at the wall and proportional to their interpenetration d_n. This force is similar to the normal force generated by two spheres in contact for the same interpenetration (Eq. 6).

$$F_w = K_n \cdot d_n = \frac{E_C \cdot R_i}{2} \cdot d_n \tag{6}$$

2.2 Geometry of the discrete elements

To account for a realistic behavior of the soil, the spheres of the initial model were combined to form non-convex elements. These spheres form a rigid body and are either interlocking or not. The non-convex shape of the elements limits the rotations of the global elements and the rolling mechanisms. To simplify their geometry, the radii of the spheres making up an element are identical. An angularity coefficient, denoted *ang*, quantifies the concave aspect of the element based on the distance d between two spheres composing an element and their radius R (Eq. 7, Fig. 1).

$$\text{ang} = \frac{d}{2 \cdot R} \tag{7}$$

The morphology of an element is defined by two parameters: the number of spheres that compose it and the angularity. The number of spheres varies from 1 to 4 (Fig. 2). Later, this number of spheres per element will be associated to the element models: model $1R$ for independent spheres, model $2R$ for axisymmetric elements comprising two spheres, models $3R$ and $4R$ for asymmetric elements made up of three and four spheres.

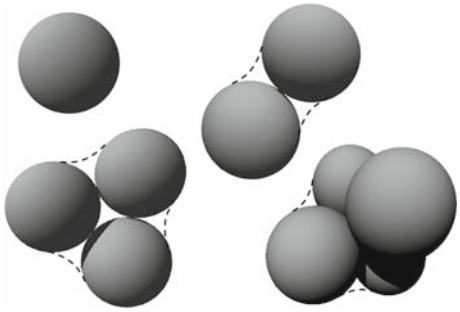

Fig. 2 Influence on the number of spheres per clumped element (1, 2, 3 and 4) on the geometry of the clumps for ang = 1

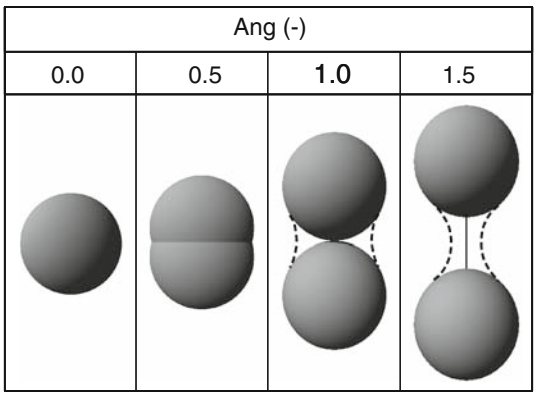

Fig. 3 Influence of angularity on the geometry of elements composed of two spheres

Angularity characterizes both the slenderness ratio and the concavity of the elements. For ang = 0, the elements are perfectly spherical and for ang = 1, the spheres of the elements are tangent (Fig. 3). For ang = 1.4, the spheres of the element have no contact with each other but can also be considered a rigid body. Depending on the sample's granulometry, limit angularity values are set such that the elements can never cross each other. The non-convexity of the element increases with the value of ang and limits the global rolling mechanisms. Usually, the microscopic angle is used to simulate a friction (that limits rotations) and the shape of the elements remain spherical or at least non-convex. Taking convexity into account enables a real aspect of the non-spherical and the roughness of natural materials to be added.

Within a granular assembly, the size of the constitutive spheres of the elements is randomly selected between radii $R_{\max}$ and $R_{\min}$. These radii depend on the size of the numerical sample and the number of elements to be studied.

2.3 Methods for 3D sample preparation

The preparation of an isotropic, homogeneous numerical sample is not easy. Currently, several methods exist for set-up. According to Bagi [47], they can be divided into two main categories.

First, there are the methods called constructive algorithms that create a sample from algorithms that are exclusively based on the geometry of the elements. These are generally used for 2D assemblies and become difficult to develop for any 3D shapes. Moreover, one cannot obtain minimum and maximum porosities for a given sample with these methods.

Second, there are the dynamic methods that are based on rearranging the granular assembly by displacing and/or increasing the size of the elements. The simplest method consists in positioning the elements by gravitational deposition, which tends to generate anisotropic assemblies. To prevent this anisotropy, Combes [48] suggests randomly mixing followed by enlarging the elements or sedimentation under a field of gravity. A number of authors [8,28,43,49,50] suggest positioning the elements in a given volume and then increasing the density of the soil by reducing the volume or enlarging the elements. These methods are particularly well adapted to random volumes and shapes and generate isotropic and homogenous samples. Chareyre and Villard [51] developed a method called radius expansion–friction decrease (REFD), which generates a precise management of the final porosity for a 2D sample. Small-size elements with micromechanical properties are generated e in a given volume, then increase in size until they exert a stress of 1 kPa on the walls. The friction is then reduced and the diameter of the elements is increased to maintain the stress on the walls until the desired porosity is achieved.

In the current study, the REFD method was used and adapted to obtain granular assembly at different states of porosity. The elements are set up randomly using a small size in a given volume so that there is no contact between two elements. The micromechanical parameters of the material needed to reproduce the macroscopic behavior are set from the beginning of the computations (stiffness and microscopic friction angle φ_μ).

The radii of the elements are increased until a mean given stress σ_0 is exerted on the walls of the volume. The porosity of the material obtained is called maximum porosity.

The microscopic friction is progressively reduced and simultaneously the radius of the elements is increased to maintain the mean stress on the walls at the value σ_0. This numerical procedure is applied until the desired porosity is obtained. If the microscopic friction reaches the null value, the porosity obtained is called minimum porosity.

After stabilizing the numerical sample the micromechanical properties of the granular assembly to be tested (φ_μ) are thus affected. This method introduces only two new parameters: the speed of element enlargement and σ_0. These parameters have only a slight influence on the final state of the sample if a sufficiently low speed at which the elements enlarge is chosen and the mean pressure remains weak enough in comparison with the confining pressure used during the numerical simulations of triaxial tests.

2.4 Determining the relative density (RD) of the numerical sample

Traditionally, when the numerical and experimental geometries of the particles are close to each other, users of discrete numerical models seek to numerically reproduce experimental porosities (e.g., elements that have a quasi-spherical shape). In the opposite case, the difference in morphology between the model's elements and the real grain assembly makes any direct comparison between the numerical and experimental porosities impossible. It is then more appropriate to attempt to make the relative densities (RD) of the granular medium studied coincide. The RD coefficient describing the state of porosity of the granular assembly studied compared to the minimum ($n_{\min}$) and maximum ($n_{\max}$) porosities is defined by Eq. 8. At maximum porosity, RD = 0% is obtained, and at minimum porosity, RD = 100%.

$$\mathrm{RD} = \frac{(n_{\max} - n) \cdot (1 - n_{\min})}{(n_{\max} - n_{\min}) \cdot (1 - n)} \tag{8}$$

The notion of relative density is rarely raised in discrete numerical simulation. However, many authors have carried out simulations using samples for loose and dense states [49,50]. In 2D, Deluzarche et al. [52] present a procedure that defines minimum and maximum porosities of a granular assembly. They created clusters of spherical elements using PFC^{2D} set up by enlargement. Maximum porosities are obtained from frictioning samples placed by gravity. Minimum porosities are obtained by the successive change in the microscopic friction angle of the elements, an isotropic compression and cycles of compaction by the walls. The intervention of gravity and the compacting procedure can, however, generate anisotropy of the sample.

The procedure adopted for this study to implement a sample with a fixed relative density is based on the method advanced by Deluzarche et al. [52] and the REFD procedure described above. For each material, the computation procedure adopted provides a first estimation to determine as defined previously the maximum and minimum porosities of the numerical sample. It is then possible to choose the porosity corresponding to the relative density desired, by reproducing the closest geometric configuration beyond the porosity sought.

3 Modeling triaxial compression tests

3.1 Principle

The numerical samples are generated in a cubic volume defined by six walls (the initial volume of the cube is 1 m^3). When the desired porosity of the sample is reached the size of the element remains constant. Thus the final size of the element is a function of the initial porosity and of the number of grains used. The element assemblies have a grain size distribution that is tight and uniform. The ratio between the largest and the smallest elements is 2.

An isotropic loading is then applied with a confining pressure $\sigma_1 = \sigma_3$ (Fig. 4). The volume of the sample decreases. After isotropic confinement, the homogeneity of the sample was observed via the isotropy of the contact distribution [49].

Finally, e triaxial compression is realized by imposing a vertical compression speed. At the same time confining pressure σ_3 is maintained constant. The confining pressure σ_1 is measured on the horizontal walls and a positive deviatoric stress q defined by Eq. 9 is calculated. The volume of the samples varies during the triaxial test.

$$q = \sigma_1 - \sigma_3 \tag{9}$$

The sample can be compared to a representative volume element when the number of elements is sufficiently high for the scattering on the macroscopic results to be sufficiently low. Figure 5 presents the macroscopic response of five different numerical samples obtained using the same numerical process. As shown on this figure, for a $2R$ model comprising 8,000 elements, the scattering on the macroscopic response of the model remains low. This shows the good reproducibility of the numerical process selected. In parallel, the influence of the number of elements on the macroscopic response is slight if assemblies larger than 8,000 elements are considered (Fig. 6). The representative volume elements are therefore modeled by 8,000 element assemblies.

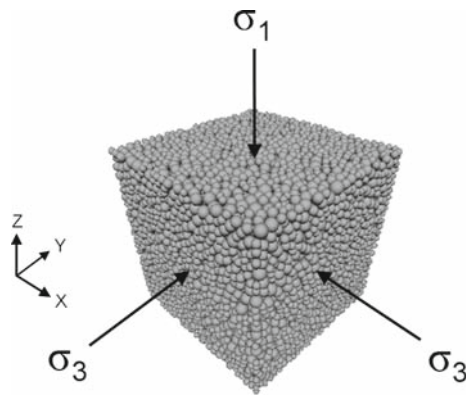

Fig. 4 Illustration of a sample (Mod. 2R, ang = 1, RD = 50%)

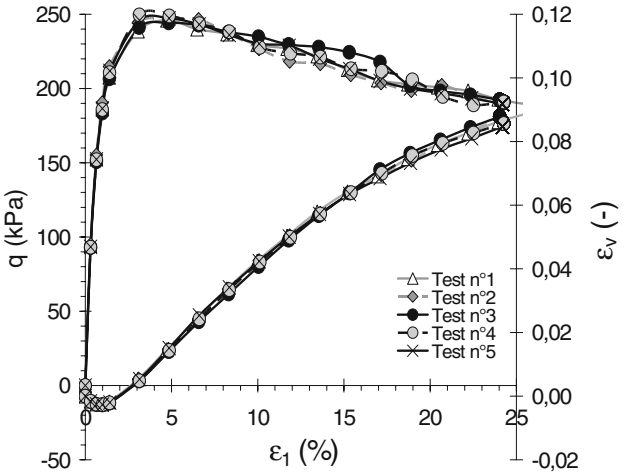

Fig. 5 Scattering of the results for the deviator and the volume strain (Mod. 2R, σ_3 = 80 kPa, ang = 1.4, RD = 60%, E_c = 300 MPa, $\alpha = 0.2$ and $\varphi_\mu = 20°$)

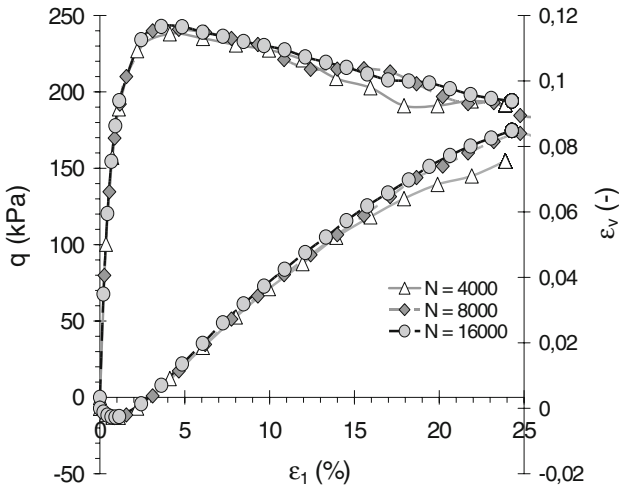

Fig. 6 Influence of the number of elements N on the deviator and the volume strain (Mod. 2R, σ_3 = 80 kPa, ang = 1.4, RD = 60%, E_c = 300 MPa, $\alpha = 0.2$ and $\varphi_\mu = 20°$)

3.2 Influence of relative density on the model's macroscopic response

The triaxial test was numerically simulated on several samples for relative densities of 0, 25, 50 and 100%. The changes in the deviator, porosity, and the number of coordinations are shown as a function of the axial strain for a 150kPa confining pressure (Figs. 7, 8, 9). The coordination number, defined as the mean number of contacts per element, is noted z. At the initial state, the densest samples are characterized by a high coordination number (Fig. 9). They generate a peak of the stress deviator and a reduction in the coordination number during triaxial compression. For an axial strain close to 20%, the stress deviators obtained at different relative densities tend toward a common value. This observation matches

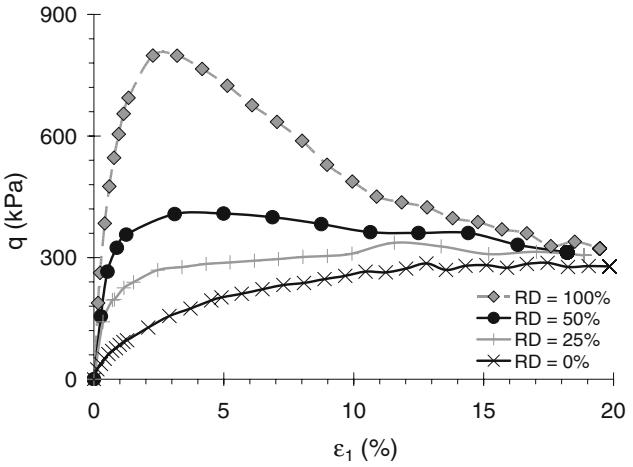

Fig. 7 Influence of relative density on the deviator (Mod. 2R, σ_3 = 150 kPa, ang = 1.4, E_c = 600 MPa, α = 1.0 and φ_μ = 30°)

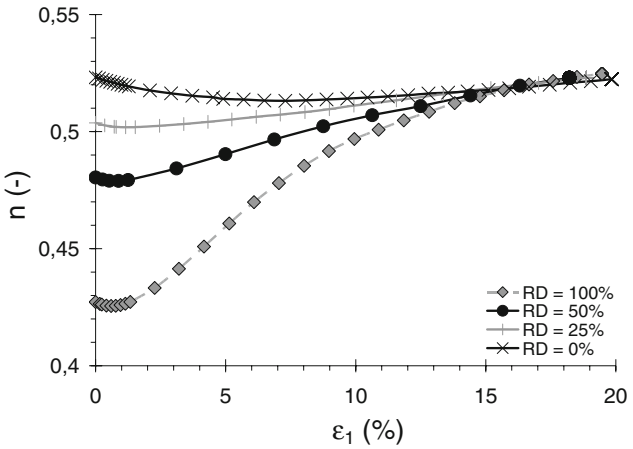

Fig. 8 Influence of relative density on porosity (Mod. 2R, σ_3 = 150 kPa, ang = 1.4, E_c = 600 MPa, α = 1.0 and φ_μ = 30°)

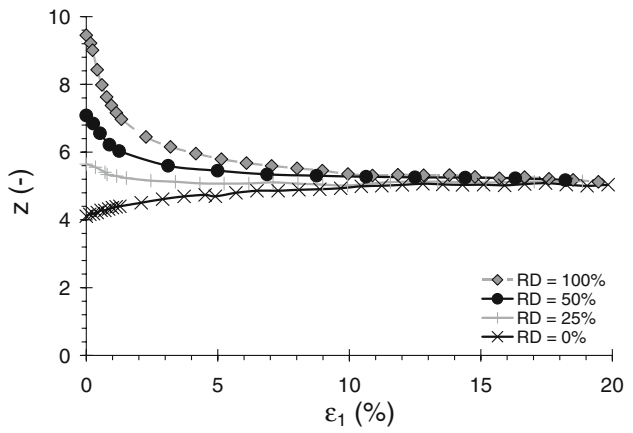

Fig. 9 Influence of relative density on the coordination number (Mod. 2R, σ_3 = 150 kPa, ang = 1.4, E_c = 600 MPa, α = 1.0 and φ_μ = 30°)

Kruyt and Rothenburg's observation [50]. Figures 7, 8 and 9 also show that the samples' porosity coordination numbers are identical for a high axial strain. The notion of critical state is therefore satisfied because the final state of a sample is not dependent on its initial relative density.

4 Micro–macro calibration procedure

The purpose of the computer model is to reproduce experimental results. This means determining the values of micromechanical and geometrical parameters of the model that provide a better correlation between numerical and experimental results (in terms of deviator curves—axial strain and volume strain—axial strain for triaxial tests). The procedure that enables an optimal set of parameters to be chosen is called the micro–macro calibration procedure. It was deduced from the results of a numerical parametric study given the influence of the main geometrical and micromechanical parameters. In order to argue the choice made to define the calibration process, the results of the parametric study are first detailed.

Since the arrangement of the elements plays an important role in the macroscopic behavior of granular assemblies, the influence of the main geometric parameters of the elements (morphology and angularity) on the minimum and maximum porosities will be presented first. Then the influence of geometric parameters on the macroscopic results obtained at a given relative density is determined. The influence of micromechanical parameters is summarized in the last part. Finally, the micro–macro procedure is deduced from the various dependencies.

4.1 Principle

To set up the procedure, the influence of the tested parameters on the model's volume stresses and strains was studied. Axial simulations were carried out on 8,000-element samples the sphere diameters of which were between R_{max} and R_{min}. The R_{max}/R_{min} ratio reflects the spread of the granulometric curve. In the following, N_s denotes the number of spheres per element and z_0 the initial coordination number. The macroscopic results of the numerical model are characterized by five parameters: E_0 the initial modulus, φ_{peak} the friction angle at its peak, φ_c the critical friction angle, υ_0 the Poisson ratio, and ψ the dilatancy angle.

4.2 Influence of the shape of the elements on the samples' minimum and maximum porosities

The numerical samples are set up at a given porosity, which, when the minimum and maximum porosities are known, can be expressed by a relative density RD required for all comparisons. The shape of the elements, which is characterized by a model of an element and an angularity, has a

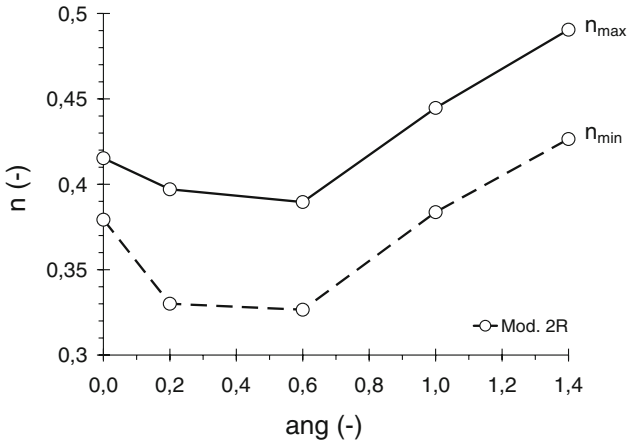

Fig. 10 Influence of angularity on minimum and maximum porosities (Mod. 2R, $E_c = 600\,\text{MPa}$, $\alpha = 0.1$ and $\varphi_\mu = 15°$)

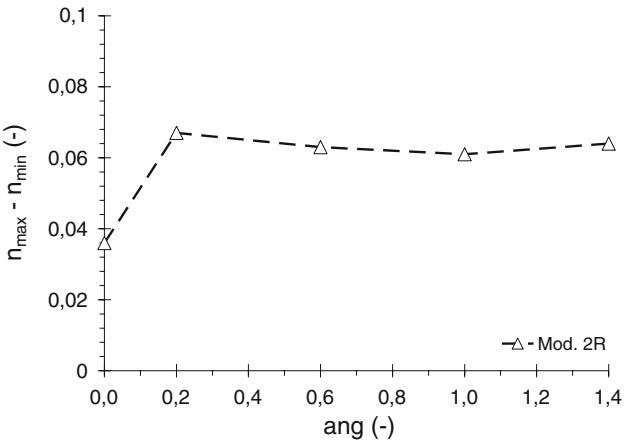

Fig. 11 Influence of angularity on the difference between maximum and minimum porosities (Mod. 2R, $E_c = 600\,\text{MPa}$, $\alpha = 0.1$ and $\varphi_\mu = 15°$)

role in the initial interlocking and arrangement of the elements. It therefore influences the different states of porosity. To determine this influence, samples made up of various angularities, then different models of elements were set up at minimum and maximum porosities according to the procedure described above. The micromechanical contact parameters are set: $E_c = 600\,\text{MPa}$, $\alpha = 0.1$ and $\varphi_\mu = 15°$.

4.2.1 Influence of angularity

Tests were conducted for five angularity values (0, 0.2, 0.6, 1 and 1.4) for the two-sphere elements ($2R$ model). The minimum and maximum porosities obtained in each case are reported in Fig. 10. It can be seen that an increase in angularity generates a reduction in minimum and maximum porosities first. Extended elements but sufficiently close in shape to a sphere allow a better filling of the void spaces. For higher angularities, the effect of the more lengthened shapes generates an increase in porosity. For angularities over 1, a volume of void space is constantly present between two spheres comprising an element; that indeed explains the porosity increases.

The difference between maximum and minimum porosities seems almost constant when the angularity is greater than 0.2 (Fig. 11). The difference in behavior obtained between a null angularity and a 0.2 angularity may be related to a high level of rolling of the spherical elements, which are constantly rearranging themselves and generate a low maximum porosity. It has been observed elsewhere that this rolling mechanism has a predominating role when microscopic friction is high and an insignificant role when friction is null. A very low angularity (0.2) would therefore suffice to limit the rolling phenomenon and make it possible to obtain minimum and maximum porosities that are almost constant for the highest levels of angularity.

Comparing the minimum porosities obtained for angularities ang $= 0$ and ang $= 1$ (Fig. 10), it can be seen that these values are very similar. For null microscopic friction, the sliding and the rolling between elements (made of two tangent inseparable spheres) is enough to obtain the same porosity as that for an assembly of spheres alone. Taking into account the contacts within spheres making up the same element, the calculation of the number of contacts per sphere reaches a value of 5.8 for ang $= 1$ and 5.6 for sphere assemblies (ang $= 0$). Both samples are therefore in a state that is very close to minimum porosity. If there is microscopic friction, the porosity is greatly modified between ang $= 1$ and ang $= 0$, so the existence of friction clearly prevents the rearranging of non-spherical elements.

4.2.2 Influence of the element model

To demonstrate the influence of the shape of the element on the minimum and maximum porosities, tests were carried out on five angularity values (0, 0.2, 0.6, 1.0 and 1.4) and for different element models ($2R$, $3R$ and $4R$ models). The minimum and maximum porosities obtained in each case are reported in Fig. 12.

It can be seen that the tendencies observed for two-sphere elements are reproduced for three- and four-sphere elements. In particular, the gap between minimum and maximum porosities is almost constant as soon as the angularity value is higher than 0.2. However, an increase in the number of spheres per element generates a reduction in the minimum and maximum porosities for an angularity of less than 0.6. In this case, the interpenetration of the spheres of a single element is better, which results in a lower global porosity. The inverse is obtained for an angularity greater than 1.0 since the pore spaces between the elements increase with the number

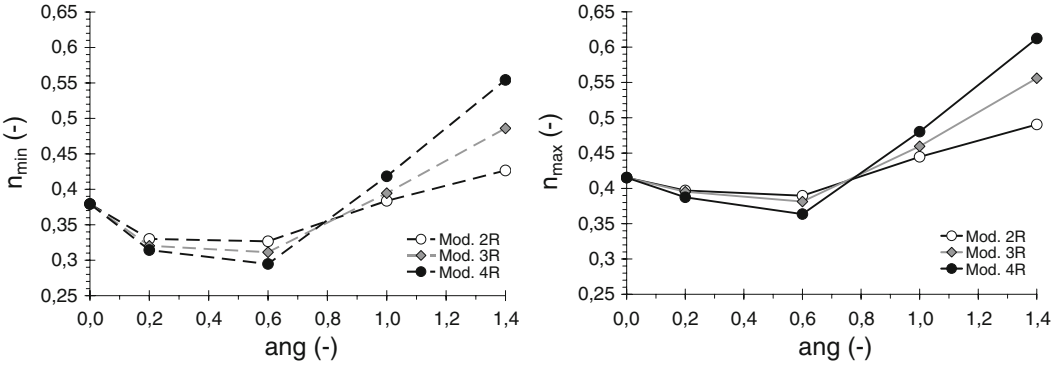

Fig. 12 Influence of the element model and angularity on minimum and maximum porosities ($E_c = 600\,\text{MPa}$, $\alpha = 0.1$ and $\varphi_\mu = 15°$)

of elements, giving a minimum porosity of the $3R$ and $4R$ models that is greater than the porosity of the $2R$ model.

As this study shows, the sample's intrinsic porosity makes it impossible to establish a direct correlation between the porosities of the numerical samples and the porosities of real soils. The minimum and maximum porosities depend to a large extent on the shape and angularity of the elements. However, the notion of relative density based on comparing the state of porosity as a function of minimum and maximum porosities is independent of the geometry of the elements. It should also be noted that for a given granular assembly of non-spherical elements, the gaps between the minimum and maximum porosities are independent of the number of spheres per element and the angularity.

4.3 Influence of element shape on the model's macroscopic results

To determine the influence of the element shape on the macromechanical behavior of granular assemblies, numerical simulations were carried out on the samples studied above. To compare the results quantitatively, these simulations were accomplished on samples with the relative density RD equal to 50% (at different initial porosities). For all these simulations, the micromechanical contact parameters remain the same ($E_c = 600\,\text{MPa}, \alpha = 0.1$ and $\varphi_\mu = 15°$) and the confining stress is 110 kPa.

4.3.1 Influence of angularity

The results obtained with the $2R$ model for several angularity values are compared in Figs. 13 and 14 (deviator q and volume variation ε_v as a function of ε_1). An increase in the deviators to the peak value and at a steady state with the angularity can be observed (Fig. 13). This is related to an improved interlocking of the elements because of the increase in concavity of the elements as a function of angularity. With the $2R$ model, the residual friction angles were 20° for null

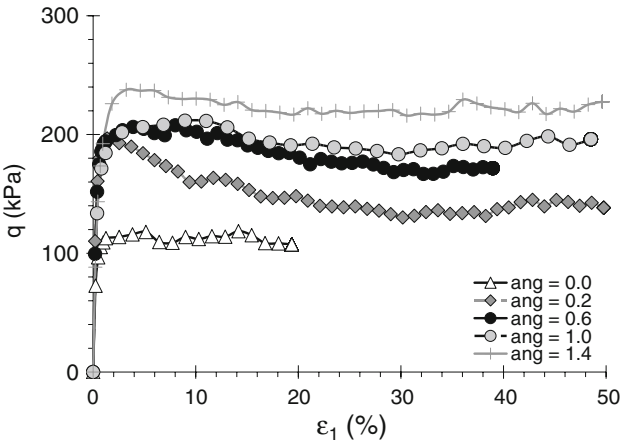

Fig. 13 Influence of angularity on the 2R model's deviator (RD = 50%, $\sigma_3 = 110\,\text{kPa}$, $E_c = 600\,\text{MPa}$, $\alpha = 0.1$ and $\varphi_\mu = 15°$)

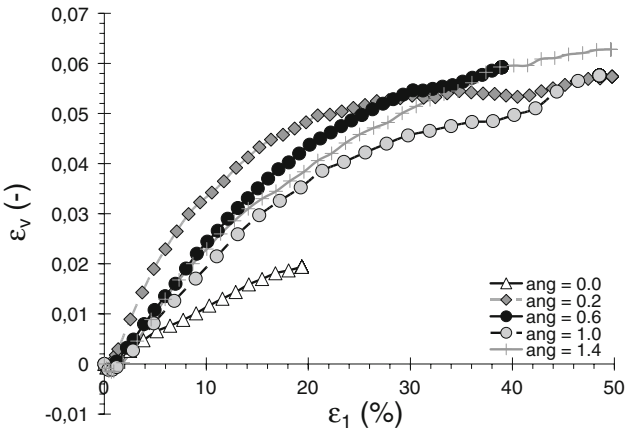

Fig. 14 Influence of angularity on the volume strain of the 2R model (RD = 50%, $\sigma_3 = 110\,\text{kPa}$, $E_c = 600\,\text{MPa}$, $\alpha = 0.1$ and $\varphi_\mu = 15°$)

angularity (perfectly spherical elements) and 28° for a 100% angularity (tangent spheres). These values remain lower than critical friction angles given in the literature for non-cohesive soils such as sands: 34°–39° for medium to fine sands of the

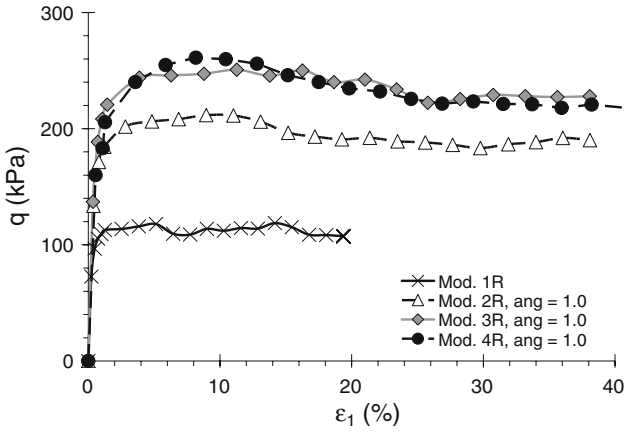

Fig. 15 Influence of the number of spheres per element on the deviator response (RD = 50%, σ_3 = 110 kPa, ang = 1, E_c = 600 MPa, α = 0.1 and φ_μ = 15°)

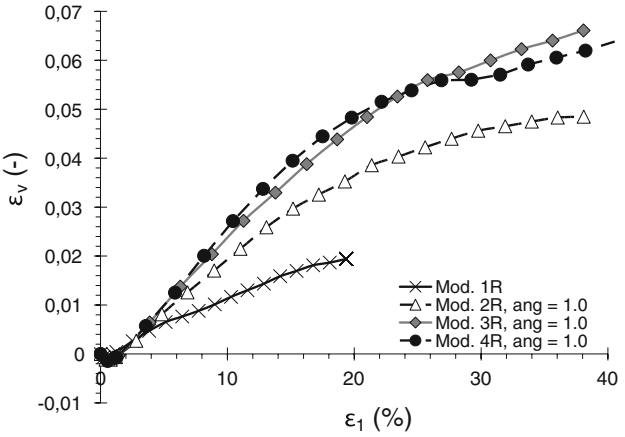

Fig. 16 Influence of the number of spheres per element on the volume strain response (RD = 50%, σ_3 = 110 kPa, ang = 1, E_c = 600 MPa, α = 0.1 and φ_μ = 15°)

Venice lagoon [53], roughly 31° for Athabasca sand [54], and from 30° to 34° for Hostun sand [55].

The influence of angularity on the volume strain curves (Fig. 14) is low for angularities greater than 0.6. The interlocking of elements generates a tendency to dilatancy that is compensated by an increase in initial porosity (Fig. 10), providing relatively similar volume variation curves depending on the axial strain.

4.3.2 Influence of the element model

To generate more realistic macroscopic behaviors of granular soils (relatively high friction angles at plasticity), one must take into consideration the more complex shaped elements (asymmetric models $3R$ and $4R$). To determine the influence of the different model elements ($1R$, $2R$, $3R$ and $4R$) on the macroscopic results of the granular assemblies, several triaxial simulations were carried out on 1.0 angularity samples. The results obtained are compared in Figs. 15 and 16. Figure 15 shows that the $2R$ model yields strengths at the peak and at plasticity that are far higher than those of the $1R$ model but lower than those produced by the $3R$ and $4R$ models results of which, in terms of deviator and volume variation (Fig. 16), are quite similar.

For a given angularity, the symmetry of the elements (perfect symmetry for the $1R$ model, rotational symmetry for the $2R$ model, and asymmetry for the $3R$ and $4R$ models) determines rolling and rotation of the elements. This seems to explain the differences in behavior observed between the different models.

4.3.3 Influence of shape on element rotation

To quantify the influence of angularity and the element model on the rolling mechanisms obtained during triaxial compression, Eq. 10 is used to define coefficient C_r. It characterizes the rotation of the elements. It is defined by the relation between the mean rotation $|\Delta\theta|$ of the elements of any sample and the mean rotation $|\Delta\theta|_{\text{ang}=0}$ of a sample made up of null-angularity elements (spherical elements). $|\Delta\theta|$ is the mean absolute rotation of the elements of a given sample calculated between 0 and 20% axial strain.

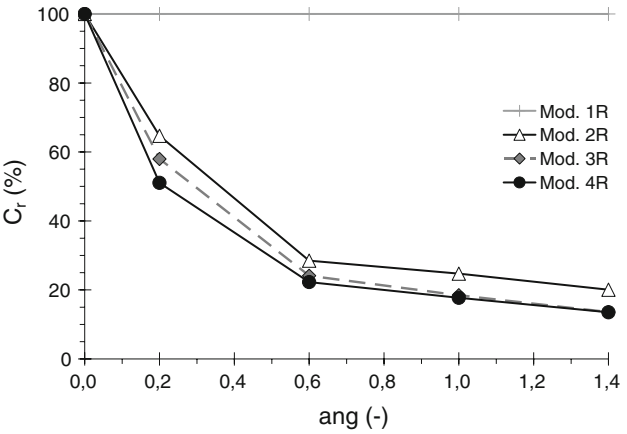

Fig. 17 Rotation coefficient as a function of angularity for the different models (RD = 50%, σ_3 = 110 kPa, E_c = 600 MPa, α = 0.1 and φ_μ = 15°)

$$C_r = \frac{|\Delta\theta|}{|\Delta\theta|_{\text{ang}=0}} \tag{10}$$

Coefficient C_r was calculated for all the numerical simulations ($1R$–$4R$ models and angularity from 0 to 1.4). Figure 17 shows that the angularity significantly reduces the rotations between the elements and that the reduction of C_r is greater for low angularities. A non-null angularity leading to an asymmetry in shape, even low, is enough to perturb the rotation mechanisms. The $3R$ and $4R$ models, the results of which are similar, limit the rotations more than

Table 1 Influence of the geometric and micromechanical parameters on the macroscopic results

	n_{max}	n_{min}	For any RD					
			z_0	φ_c	ν_0	E_0	φ_{peak}	ψ
R_{max} / R_{min}	□	□	□	-	-	-	-	□
N_s	x	x	□	□	□	-	□	□
ang	x	x	x	□	□	x	□	x
α	□	-	□	-	□	□	□	□
E_c	-	-	□	-	-	□	□	□
$\varphi_\mu > 15°$	□	-	□	-	-	-	□	□

□ : Clear dependence
x : Unclear dependence
- : No dependence on parameter

the $2R$ model does, which allows rotations around the symmetry axis. In view of the curves presented, the evaluation of the mean rotation of the elements clearly shows that the strength of a sample is highly dependent on the rotation of its elements.

It can be concluded that to obtain realistic friction angles for soil behavior at plasticity, the shape of asymmetrical and angular elements must be taken into account. These shapes limit the elements rolling among each other and make it possible to increase the global strength of the material. When a certain asymmetry is reached ($3R$ and $4R$ models), the results vary little, whether in terms of strength or element rolling. To minimize the number of spheres and the computation time, the $3R$ model is preferred over the $4R$ model.

4.4 Procedure for calibrating micromechanical and geometric parameters

The results of the parametric study show the influence of angularity and the element model on the model's macroscopic results. They establish a qualitative relation between these parameters (ang and N_s) and the macroscopic parameters reproduced (φ_c, φ_{peak}, E_0 and υ_0). Table 1 summarizes these trends and presents the influence that the micromechanical parameters have on the macroscopic parameters (E_c, α and φ_μ) for φ_μ greater than 15°. It should be noted that:

- The critical friction angle φ_c depends, for the most part, on the angularity and the element model. This is in agreement with the simulation results on 2D models found by Mahboubi [49]. Kruyt and Rothenburg [50] which also showed little change in the critical friction angle φ_c with the microscopic friction angle φ_μ for values greater than 15°.
- The Poisson ratio υ_0 decreases when the ratio between the tangential stiffness and normal stiffness α increases. The same observation was made in Collop et al. [56].
- The initial modulus E_0 is independent of the microscopic friction angle φ_μ.
- The friction angle at the peak φ_{peak} and the dilatancy angle ψ both depend on the angularity and all the micromechanical contact parameters.

The calibration procedure consists in determining the set of micromechanical parameters that are best adapted to reproduce the experimental behavior of the material to be modeled. The different steps of this procedure are summarized in Fig. 18.

The R_{max}/R_{min} ratio and the element model were initially set in order to limit the number of spheres to a reasonable value (elements of neighboring sizes, limited number of spheres per element). The confining stress adopted corresponds to the experiment's confining stress. Initially, all of the model's parameters to be set (ang, α, E_c, φ_μ) were chosen arbitrarily by the user with $\varphi_\mu > 15°$. For this set of parameters, the minimum and maximum porosities are obtained by the numerical process described in part 2.3. Consequently, a sample is created with a relative density resembling the experimental sample. A triaxial test is carried out on this sample and the model's response is compared to the experimental curves to initiate the calibration phase. When one of the model's parameters is modified, a new search for minimum and maximum porosities is carried out, except for the calibration of E_c, which has no influence on these porosities (Table 1).

Four successive steps are necessary to calibrate the model (Fig. 18):

(a) If the model's critical friction angle is greater than the critical friction angle obtained experimentally, the angularity of the elements is reduced. In the opposite case, it is increased. If the material's critical friction angle cannot be reproduced by the $2R$ model, the $3R$ model is used. When the critical friction angle is restored cor-

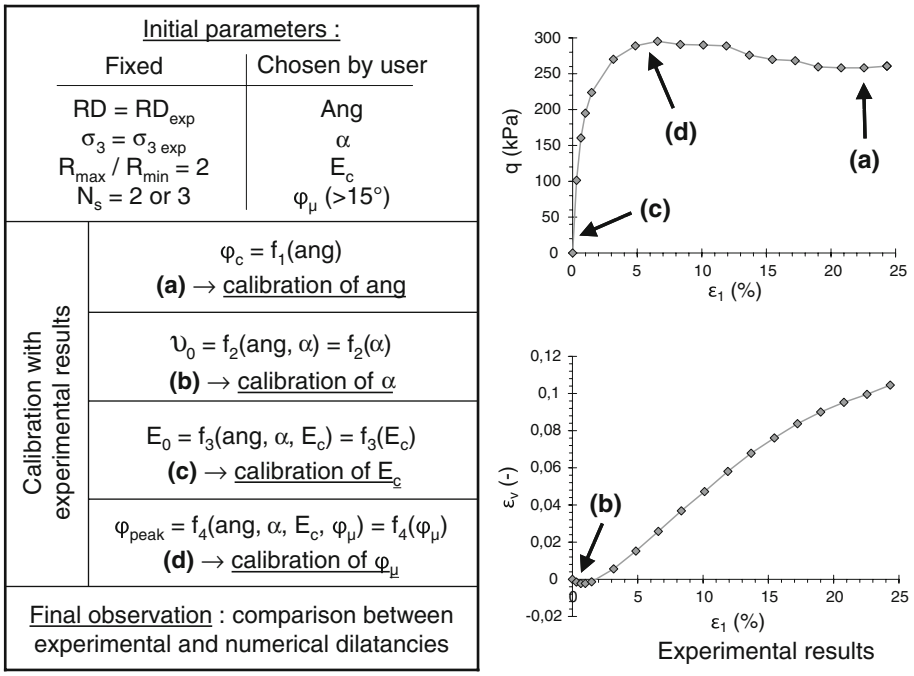

Fig. 18 Parameter calibration procedure for the model based on experimental data and results

rectly for a given angularity value, the calibration process is continued by step b.

(b) Similarly, parameter α is calibrated to come as close as possible to the Poisson ratio of the material to be modeled. The parameter α does not influence the critical friction angle obtained (Table 1) and therefore does not implicate the calibration of ang.

(c) E_c is determined so that the model can reproduce as accurately as possible the experimental initial modulus E_0. This modification does not change the preceding calibrations, as can be noted in Table 1.

(d) The microscopic friction angle φ_μ is adjusted so that the numerical model approaches the friction angle at the peak φ_{peak} of the material to be modeled. It was shown above that φ_μ has little influence on the residual friction angle for a value greater than 15°.

Finally, the dilatancy angle obtained by the numerical model is compared to the angle in the experiment. Testing new shapes of elements can be undertaken if necessary for a better calibration of the model (cf. Sect. 5).

In conclusion, the geometric and micromechanical parameters (ang, α, E_c, φ_μ) are determined successively analogous to the macromechanical parameters of the material to be simulated (φ_c, υ_0, E_0, φ_{peak}). At the end of the simulations conducted for a $2R$ element model, if the critical friction angle is too low or the dilatancy angle ψ does not correspond to the experimental value, a $3R$ element (or $4R$) model must be tested. In this case, all of the parameters must be calibrated again.

5 Application to tests on real sand

This application was tested as part of a research project financed by the Rhône-Alpes region of France (GeoDis project). The project's objectives were to compare various numerical models based on the DEM and to analyze their ability to reproduce experimental results. This required experimental tests carried out on a Ticino sand provided by the Politecnico di Milano, Milan, Italy, a partner in the project. Part of these results, from V. Ghionna and D. Porcino, are used in this section.

5.1 Description of the Ticino sand

Drained axisymmetric triaxial compression tests were conducted on Ticino sand for two ranges of relative density (data provided by V. Ghionna and D. Porcino, Università Mediterranea di Reggio-Calabria, Italy). Figure 19 summarizes all the geometric characteristics of the material tested: the shape of the grains (morphology, sphericity, mineralogy, specific gravity G_s), granulometry (granulometric curve, uniformity coefficient c_u), and the minimum γ_{min} and maximum γ_{max} densities.

The objective of the numerical study was to develop a model that could reproduce the experimental behavior of sand for various densities and confining pressures.

The model will be calibrated on the basis of a single experimental trial carried out on a sample with a relative density equal to 47% (the authors wish to come closer to 50%) and for a 109-kPa confining pressure. The micromechanical and geometric parameters of the model thus calibrated will be

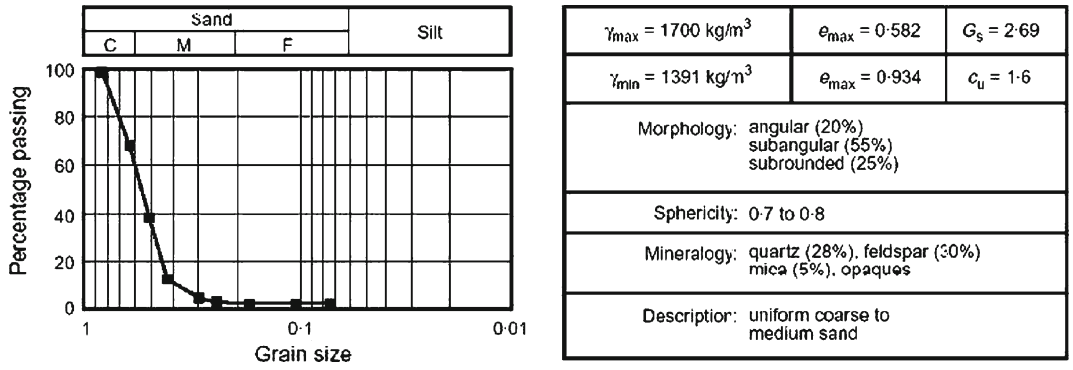

Fig. 19 Index properties of Ticino sand (V. Ghionna and D. Porcino)

Table 2 Comparison of the parameters obtained for the 2R and 3R models

	Parameters				Porosities		
	ang (–)	α (–)	E_c (MPa)	φ_μ (°)	n_{max} (RD = 100%)	n_0 (RD = 47%)	n_{min} (RD = 0%)
Mod. 2R	1.40	0.1	1,100	25	0.504	0.472	0.427
Mod. 3R	1.30	0.1	800	19	0.550	0.519	0.479

fixed. The predictive results of the numerical model will then be compared with the experimental results obtained in different trial conditions for density and confining pressure (relative density 73% (the authors wish to come closer to 75%), confining pressure 100, 200 and 300 kPa).

5.2 Calibration of the model's micromechanical properties

Two element models were tested: the $2R$ model made up exclusively of two-sphere elements and the $3R$ model made up exclusively of three-sphere elements. To optimize computation time, the granulometry of the numeric soil was defined by a R_{max}/R_{min} ratio of 2. The calibration of the micromechanical and geometric parameters of the models is carried out according to a protocol established earlier based on experimental results from a relative density sample equal to 47% and for a pressure confinement of 109 kPa.

The reduced strain rate, defined by Roux [57], quantifies the ratio of inertia forces and the imposed forces. Its value, proportional to the compression speed, is low for a quasistatic regime and high for a dynamic regime. During the tests carried out, the reduced strain rate is between 1.7×10^{-4} and 1.8×10^{-4}. The maximum variation of σ_3 compared to the mean reference value is 0.69%.

Table 2 presents the micromechanical parameters for the calibration for each of the models. The numerical results obtained for the $2R$ and $3R$ models are compared with the experimental curves in Figs. 20 and 21.

The $2R$ model makes it possible to come close to the deviator obtained experimentally (Fig. 20). However the dilatancy obtained numerically is much greater. The $3R$ model allows a

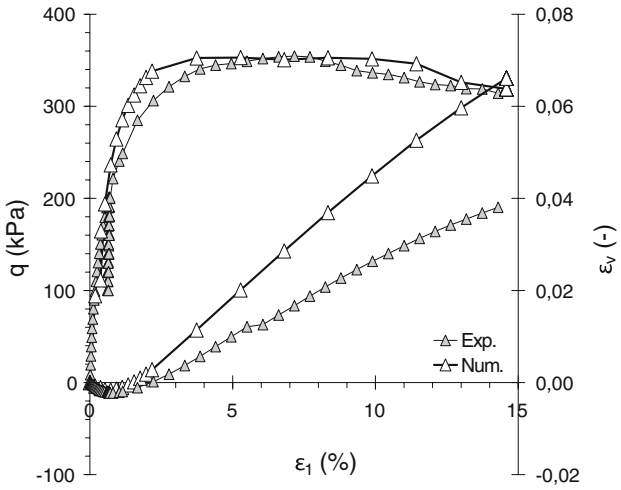

Fig. 20 Comparison of the experimental and numerical reference curves for the 2R model (RD = 47%)

better approach of the volume strain curve (Fig. 21). The sample is less dilatant because the microscopic friction angle that enables calibration is lower (Table 2). The number of spheres per element plays an important role in the micromechanical parameter calibration process. At equal parameter values, the $3R$ model reduces element rotation while the $2R$ model does not. This generates an increase in strength, which is compensated during calibration by a reduction in the angularity and the microscopic friction angle. The $3R$ model is preferred to the $2R$ model in defining the calibration parameters. Finally, Fig. 21 shows that the $3R$ model does not correctly reproduce the elastic modulus characterizing the elastic loading

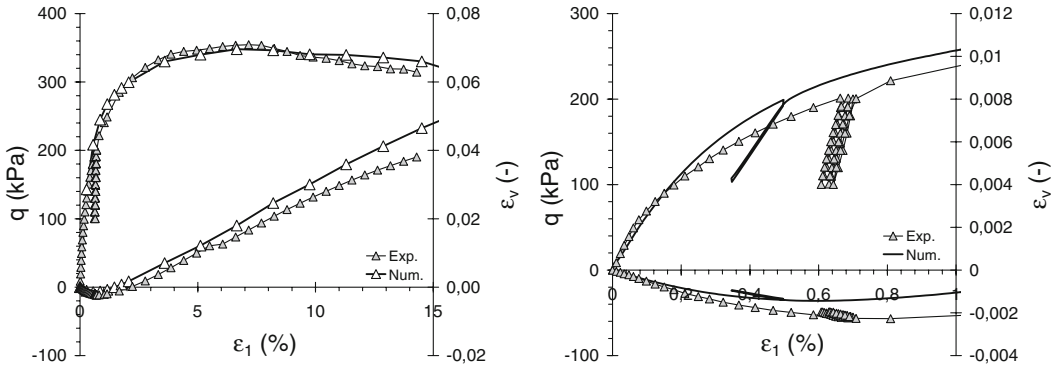

Fig. 21 Comparison of the experimental and numerical reference curves for the 3R model, with enlargement of the initial phase

Table 3 Relative densities obtained for the experimental and numerical trials at various confining stresses (%)

	RD (%)	
Confining pressure σ_3 (kPa)	Experimental (Exp.)	Numerical Mod. 3R (Num.)
109–110 (calibration test)	47	47
99–100	72	72
200	74	75
300	75	76

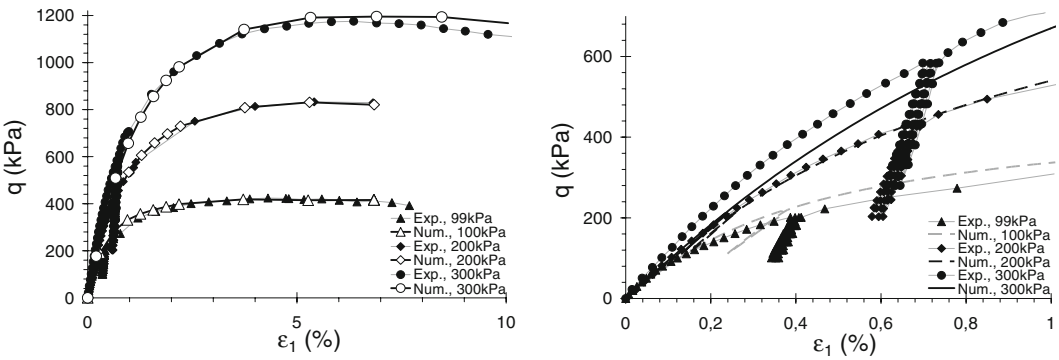

Fig. 22 Changes in the deviators obtained experimentally and numerically for the 3R model, with enlargement of the initial phase

and unloading phases of the reference soil in the domain of low axial strains (<1%).

5.3 Comparison between the numerical model and the experimental results

The 3*R* model was subjected to three triaxial compression tests for a relative density of roughly 73% and confinement stresses of 100, 200 and 300 kPa corresponding to the experimental values (Table 3). The numerical and experimental results were compared for the three trials: Fig. 22 shows the changes in the deviators and Fig. 23 the changes in volume strains.

The model reproduces the experimental deviator curves for various confining pressures (Fig. 22). For a low axial strain, as in the experiment, the model generates an increase in the initial modulus with the confining stress. However, it can be seen that the moduli of the unloading/reloading cycles are numerically identical to the initial modulus while experimentally they are greater.

The volume strain curves obtained by the model come close to the experimental curves (Fig. 23). The contraction phases (negative volume strains) are accurately simulated overall. However, certain differences between the model and the experiment in the dilatancy phase (positive volume strains) can be noted, particularly beginning with a 4% axial strain for the trial confined to 99 kPa. It is thought that these differences are related to measurement imprecisions even though no information is available on the scattering of the experimental results. Be that as it may, the slopes of the volume strain curves during the dilatancy phase are correctly reproduced by the numerical model.

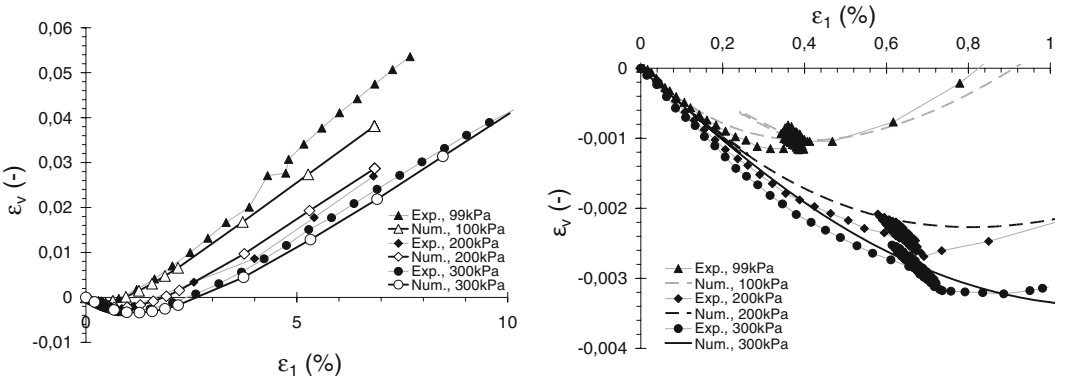

Fig. 23 Changes in the volume strains obtained experimentally and numerically for the 3R model, with enlargement of the initial phase

6 Conclusion

This study shows that the use of a simplified numerical model based on the DEM, enables the reproduction of the macroscopic behavior of a granular material without it being necessary to describe the granular structure perfectly and or take into consideration the complexity of the shape of the grain. In this study, discrete elements made up of interlocked or non-interlocked spheres were used. These elements have non-convex shapes, very different from the real shape of grains, but which enable a high level of interlocking and which limit rotations within the granular assembly. Several element shapes were tested and showed that an element asymmetry is required to account for the high residual friction angle values obtained during an axisymmetric triaxial compression. In practice, two- or three-element clusters are enough to create asymmetry thereby coming sufficiently close to the behavior of a real material.

Since the shapes of the numerical elements are remote from the real shapes, the intrinsic porosities of the numerical and experimental samples cannot be directly compared. To describe the compactness of the numerical samples, the notion of relative density was introduced. This was established based on the minimum and maximum porosities obtained using a precise and reproducible computation procedure. Under these conditions, it was shown that the numerical model, once it had been calibrated, was capable of reproducing the experimental results of the triaxial tests on sands of different relative densities and under different confining stresses. It should be emphasized that the micromechanical and geometrical parameters were calibrated based on a single experimental test according to a clearly established protocol.

It should also be noted that under these conditions, the numerical model is capable of closely reproducing the behavior of non-cohesive soils in the elastic, contraction, and dilatancy phases and at the critical state. The notion of relative density is relevant because the numerical and experimental results obtained at different relative densities correlate very well.

The model thus defined provides the opportunity for a quantitative study of the phenomena controlled by the density of a granular material. It will be used to characterize the behavior of composite materials such as heterogenous materials with large elements or for reconstituted materials such as sand–tire mixtures used for their dissipative powers in protective barriers against rockfall. To test the computation methodology under other stresses, various types of trials will be modeled, such as direct shearing tests. The results of simulations will again be compared to experimental results.

Acknowledgments The authors would like to acknowledge the support of the GeoDis research project, financed by the Rhône-Alpes region of France, for the valuable discussions related to this study: the LTDS Laboratory (Ecole Centrale de Lyon), the LMGC Laboratory (University Montpellier II), the CEMAGREF (Grenoble) and the Politecnico di Milano.

References

1. Chien, L.-K., Oh, Y.-N., Chang, C.-H.: Effects of fines content on liquefaction strength and dynamic settlement of reclaimed soil. Can. Geotech. J. **39**, 254–265 (2002)
2. Chang, M.-F., Yu, G., Na, Y.-M., Choa, V.: Evaluation of relative density profiles of sand fill at a reclaimed site. Can. Geotech. J. **43**, 903–914 (2006)
3. Yoon, Y.W., Cheon, S.H., Kang, D.S.: Bearing capacity and settlement of tire-reinforced sands. Geotext. Geomembr. **22**, 439–453 (2004)
4. Brandl, H., Blovsky, S.: Protective barriers against rockfall. In: Floss, R., Bräu, G. (eds.) Geotechnical Engineering with Geosynthetics, Eurogeo 3, Munich, Germany, 01–03 March 2004, pp. 95–100 (2004)
5. Cundall, P.A., Strack, O.D.L.: A discrete numerical modelling method for granular assemblies. Geotechnique **29**(1), 47–65 (1979)
6. Le Hello, B., Villard, P., Nancey, A., Delmas, P.: Coupling finite elements and discrete elements methods, application to reinforced embankment by piles and geosynthetics. In: Schweiger, H.F. (ed.) Numerical Methods in Geotechnical Engineering, 6th European

Conference, Graz, Austria, 06–08 September 2006, pp. 843–848 (2006)
7. Gotteland, P., Lambert, S., Salot, C., Gras, V.: Investigating the strength characteristics of tyre chips–sand mixtures for geo-cellular structure engineering. In: International Workshop on Scrap Tyre Derived Geomaterials—Opportunities and Challenges, Yokosuka, Japan, 23–24 March 2007, for publication (2007)
8. Achmus, M., Abdel-Rahman, K.: The influence of "up-scaling" on the results of particle method calculations of non-cohesive soils. In: Konietzky, H. (ed.) Numerical Modeling in Micromechanics via Particle Methods, Proceedings of the First International PFC Symposium, Gelsenkirchen, Germany, 6/7 November 2002, pp. 183–187 (2003)
9. Matsushima, T., Saomoto, H.: Discrete element modeling for irregularly-shaped sand grains. In: Proceedings of NUMGE2002: Numerical Methods in Geotechnical Engineering, Paris, France, 4–6 September 2002, pp. 239–246. Presses de l'ENPC, Paris (2002). ISBN2-85978-362-8
10. Ting, J.M., Khwaja, M., Meachum, L.R., Rowell, J.D.: An ellipse-based discrete element model for granular materials. Int. J. Numer. Anal. Methods Geomech. **17**, 603–623 (1993)
11. Ng, T.T.: Numerical simulations of granular soil using elliptical particles. Comput. Geotech. **16**:153–169 (1994)
12. Ting, J.M., Meachum, L.R., Rowell, J.D.: Effect of particle shape on the strength and deformation mechanisms of ellipse-shaped granular assemblages. Eng. Comput. **12**, 99–108 (1995)
13. Ouadfel, H., Rothenburg, L.: An algorithm for detecting inter-ellipsoid contacts. Comput. Geotech. **24**(4), 245–263 (1999)
14. Rothenburg, L., Kruyt, N.P.: Critical state and evolution of coordination number in simulated granular materials. Int. J. Solids Struct. **41**, 5763–5774 (2004)
15. Mirghasemi, A.A., Rothenburg, L., Matyas, E.L.: Numerical simulations of assemblies of two-dimensional polygon-shaped particles. Soils Found. **37**(3), 43–52 (1995)
16. Matuttis, H.G., Luding, H.G., Hermann, H.J.: Discrete element simulations of dense packings and heaps made of spherical and non-spherical particles. Powder Technol. **109**, 278–292 (2000)
17. Alonso-Marroquin, F., Hermann, H.J.: Calculation of the incremental stress–strain relation of a polygonal packing. Phys. Rev. E **66**, 022130 (2002)
18. Nouguier-Lehon, C., Cambou, B., Vincens, E.: Influence of particle shape and angularity on the behaviour of granular materials: a numerical analysis. Int. J. Numer. Anal. Meth. Geomech. **27**(14), 1207–1226 (2003)
19. Nouguier-Lehon, C., Vincens, E., Cambou, B.: Structural changes in granular materials: the case of irregular polygonal particles. Int. J. Solids Struct. **42**, 6356–6375 (2005)
20. Alonso-Marroquin, F., Luding, S., Hermann, H.J., Vardoulalis, I.: Role of anisotropic in the elastoplastic response of a polygonal packing. Phys. Rev. E **71**(5), 051304 (2005)
21. Azema, E., Radjai, F., Peyroux, R., Saussine, G.: Force transmission in a packing of pentagonal particles. Phys. Rev. E **76**(1), 011301 (2007)
22. Williams, J.R., Pentland, A.P.: Superquadrics and modal dynamics for discrete elements in interactive design. Eng. Comput. **9**, 115–127 (1992)
23. Mustoe, G.G.W., Miyata, M.: Material flow analyses of non-circular shaped granular media using DEM. J. Eng. Mech. **127**(10), 1017–1026 (2001)
24. Potapov, A.V., Campbell, C.S.: A fast model for the simulation of non-round particles. Granul. Matter **1**, 9–14 (1998)
25. Emeriault, F.: Anisotropic elasticity of granular assemblies with ellipsoidal elements. In: Mechanics of Deformation and Flow of Particulate Materials, ASCE. Evanston, Illinois, pp. 47–61 (1997)
26. Ashmawy A.H., Sukumaran B., Hoang V.V.: Evaluating the influence of particle shape on liquefaction behaviour using discrete element modelling. In: Proceedings of the 13th International Offshore and Polar Engineering Conference (ISOPE, Honolulu), vol. 2, pp. 542–549 (2003)
27. Sallam, A.M.: Studies on modeling angular soil particles using the discrete element method. Thèse: Philosophie: University of South Florida, 228p (2004)
28. Emeriault, F., Claquin, C.: Statistical homogenization for assemblies of elliptical grains: effect of the aspect ratio and particle rotation. Int. J. Solids Struct. **41**, 5837–5849 (2004)
29. Li, L., Holt, R.M.: Approaching real grain shape in the simulation of sandstone using DEM. In: Garcia-Rojo, R. et al. (eds.) Powders and Grains, Proceedings of the 5th International Conference on Micromechanics of Granular Media, Stuttgart, Germany, 18–22 July 2005, pp. 1369–1373 (2005)
30. Lin, X., Ng, T.T.: A three dimensional discrete element model using arrays of ellipsoids. Geotechnique **47**(2), 319–329 (1997)
31. Ng, T.T.: Fabric evolution of ellipsoidal arrays with different particle shapes. J. Eng. Mech. **127**(10), 994–999 (2001)
32. Kuhn, M.R., Bagi, K.: Contact rolling and deformation in granular media. Int. J. Solids Struct. **41**(21), 5793–5820 (2004)
33. Ng, T.T., Petrakis, E.: Triaxial test simulations with discrete element method and hydrostatic boundaries. J. Eng. Mech. **130**(10), 1188–1194 (2004)
34. Cundall, P.A.: Formulation of a three-dimensionnal distinct element model-part I: a scheme to detect and represent contacts in a system composed of many polyhedral blocks. Int. J. Rock Mech. Min. Sci. Geomech. (1988) (Abstract)
35. Saussine, G., Moreau, J.J., Dubois, F., Cholet, C., Bohatier, C., Gautier, P.E.: Modeling ballast behavior using a three-dimensional polyhedral discrete element method. In: XXI International Congress of Theoretical and Applied Mechanics, Warsaw, Poland, August 15–21 (2004)
36. Zhao, D., Nezami, E.G., Hashash, M.A., Ghaboussi, J.: Three-dimensional discrete element simulation for granular materials. Eng. Comput. **23**(7), 749–770 (2006)
37. Lu, M., McDowell, G.R.: The importance of modelling ballast particle shape in the discrete element method. Granul. Matter **9**, 69–80 (2007)
38. Jensen, R.P., Bosscher, P.J., Plesha, M.E., Edil, T.B.: DEM simulations of granular media—structure interface: effects of surface roughness and particle shape. Int. J. Numer. Anal. Meth. Geomech. **23**, 531–547 (1999)
39. Jensen, R.P., Edil, T.B., Bosscher, P.J., Plesha, M.E., Kahla, N.B.: Effect of particle shape on interface behavior of DEM simulated granular materials. Int. J. Geomech. **1**(1), 1–19 (2001)
40. Katzenbach, R., Schmitt, A.: Micromechanical modeling of granular materials under triaxial and oedometric loading. In: Shimizu, Y. et al. (eds.) Numerical Modeling in Micromechanics via Particle Methods, Proceedings of the 2nd International PFC Symposium, Kyoto, Japan, October 2004, pp. 313–322 (2004)
41. O'sullivan, C., Bray, J.D.: The importance of accurately capturing particle geometry in DEM simulations. In: Garcia-Rojo, R. et al. (eds.) Powders and grains, Proceedings of the 5th International Conference on Micromechanics of Granular Media, Stuttgart, Germany, 18–22 July 2005, pp. 1333–1337 (2005)
42. Bertrand, D., Gotteland, P., Lambert, S., Nicot, F., Derache, F.: Multi-scale modelling of cellular geo-composite structure under localized impact. Revue Européenne de Genie Civil **10**(3), 309–322 (2006)
43. Matsushima, T.: Effect of irregular grain shape on quasi-static shear behavior of granular assembly. In: Garcia-Rojo, R. et al. (eds.) Powders and Grains, Proceedings of the 5th International Conference on Micromechanics of Granular Media, Stuttgart, Germany, 18–22 July 2005, pp. 1319–1323 (2005)
44. Calvetti, F., Viggiani, G., Tamagnini, C.: Micromechanical inspection of constitutive modelling. In: Viggiani, G. (ed.) Constitutive

Modelling and Analysis of Boundary Value Problems in Geotechnical Engineering, Napoli, Italy, 22–24 April 2003, pp. 187–216 (2003)
45. Iwashita, K., Oda, M.: Micro-deformation mechanism of shear banding process based on modified distinct element method. Powder Technol. **109**, 192–205 (2000)
46. Donze, F., Magnier, S.A.: Formulation of a three-dimensional numerical model of brittle behavior. Geophys. J. Int. **122**, 790–802 (1995)
47. Bagi, K.: An algorithm to generate random dense arrangements for discrete element simulations of granular assemblies. Granul. Matter **7**, 31–43 (2005)
48. Combe, G.: Mécanique des Matériaux Granulaires et Origines Microscopiques de la Déformation. LCPC, Paris (2002)
49. Mahboubi, A., Ghaouti, A., Cambou, B.: La simulation numérique discrète du comportement des matériaux granulaires. Revue Française de Géotechnique **76**, 45–61 (1996)
50. Kruyt, N.P., Rothenburg, L.: Strength, dilatancy, energy and dissipation in quasi-static deformation of granular materials. In: Garcia-Rojo, R. et al. (eds.) Powders and Grains, Proceedings of the 5th International Conference on Micromechanics of Granular Media, Stuttgart, Germany, 18–22 July 2005, pp. 251–255 (2005)
51. Chareyre, B., Villard, P.: Discrete element modeling of curved geosynthetic anchorages with known macro-properties. In: Konietzky, H. (ed.) Numerical Modeling in Micromechanics via Particle Methods, Proceedings of the First International PFC Symposium, Gelsenkirchen, Germany, 6/7 November 2002, pp. 197–203 (2003)
52. Deluzarche, R., Cambou, B., Fry, J.J.: Modeling of rockfill behaviour with crushable particles. In: Konietzky, H. (ed.) Numerical Modeling in Micromechanics via Particle Methods, Proceedings of the First International PFC Symposium, Gelsenkirchen, Germany, 6/7 November 2002, pp. 219–224 (2003)
53. Cola, S., Simonini, P.: Mechanical behavior of silty soils of the Venice lagoon as a function of their grading characteristics. Can. Geotech. J. **39**, 879–893 (2002)
54. Samieh, A.M., Wong, R.C.K.: Modelling the responses of Athabasca oil sand in triaxial compression tests at low pressure. Can. Geotech. J. **35**, 395–406 (1998)
55. Lancelot, L., Shahrour, I., Al Mahmoud, M.: Failure and dilatancy properties of sand at relatively low stresses. J. Eng. Mech. **132**(12), 1396–1399 (2006)
56. Collop, A.C., McDowell, G.R., Lee, Y.W.: Modelling dilation in an idealised asphalt mixture using discrete element modelling. Granul. Matter **8**, 175–184 (2006)
57. Roux, J.-N.: The nature of quasistatic deformation in granular materials. In: Garcia-Rojo, R. et al. (eds.) Powders and Grains, Proceedings of the 5th International Conference on Micromechanics of Granular Media, Stuttgart, Germany, 18–22 July 2005, pp. 261–265 (2005)